Received 15 September 2022
Revised 2 November 2022
Accepted 2 November 2022

Parameter identification for MTPA control based on a nonlinear d-q dynamic IPMSM model

Mitja Garmut
Faculty of Electrical Engineering and Computer Science, Institute of Electrical Power Engineering, University of Maribor, Maribor, Slovenia

Simon Steentjes
Hilti Entwicklungsgesellschaft GmbH, Kaufering, Germany, and

Martin Petrun
Faculty of Electrical Engineering and Computer Science, Institute of Electrical Power Engineering, University of Maribor, Maribor, Slovenia

Abstract

Purpose – Small highly saturated interior permanent magnet- synchronous machines (IPMSMs) show a very nonlinear behaviour. Such machines are mostly controlled with a closed-loop cascade control, which is based on a d-q two-axis dynamic model with constant concentrated parameters to calculate the control parameters. This paper aims to present the identification of a complete current- and rotor position-dependent d-q dynamic model, which is derived by using a finite element method (FEM) simulation. The machine's constant parameters are determined for an operation on the maximum torque per ampere (MTPA) curve. The obtained MTPA control performance was evaluated on the complete FEM-based nonlinear d-q model.

Design/methodology/approach – A FEM model was used to determine the nonlinear properties of the complete d-q dynamic model of the IPMSM. Furthermore, a fitting procedure based on the nonlinear MTPA curve is proposed to determine adequate constant parameters for MTPA operation of the IPMSM.

Findings – The current-dependent d-q dynamic model of the machine models the relevant dynamic behaviour of the complete current- and rotor position-dependent FEM-based d-q dynamic model. The most adequate control response was achieved while using the constant parameters fitted to the nonlinear MTPA curve by using the proposed method.

Originality/value – The effect on the motor's steady-state and dynamic behaviour of differently complex d-q dynamic models was evaluated. A workflow to obtain constant set of parameters for the decoupled operation in the MTPA region was developed and their effect on the control response was analysed.

Keywords IPMSM, MTPA, d-q dynamic model

Paper type Research paper

COMPEL - The international journal for computation and mathematics in electrical and electronic engineering
Vol. 42 No. 4, 2023
pp. 846-860
Emerald Publishing Limited
0332-1649
DOI 10.1108/COMPEL-09-2022-0331

This work was supported by the Slovenian Research Agency (ARRS) under Project P2-0115 and Project J7-3152.

1. Introduction

Small interior permanent magnet- synchronous machines (IPMSMs) with high power-to-weight ratios behave very nonlinear, due to the slotting effect, permanent magnets, cross coupling, cross saturation and very saturated magnetically nonlinear iron core (Hadžiselimović *et al.*, 2007; Liu *et al.*, 2016). As such machines are generally controlled by using linear closed-loop cascade control, which is based on the constant concentrated parameter d-q dynamic model, adequate control parameters have to be identified (Rafaq and Jung, 2020; Zhu *et al.*, 2021; Lu *et al.*, 2022). Different complexity levels with different dependencies of the d-q models were evaluated by Pouramin *et al.* (2015), Stumberger *et al.* (2003), Michalski *et al.* (2019) and Weidenholzer *et al.* (2013).

The discussed effects can be simulated by using a finite element method (FEM) model, which was the basis for developing a complete current- and position-dependent nonlinear d-q dynamic model (Fontana and Bianchi, 2020; Müller *et al.*, 2022). This model was composed of various terms and dependencies, which model different nonlinear effects. By evaluating each of those effects, we analysed which of the terms and dependencies have a significant influence on the machine's behaviour in respect to speed control. The simplest model that models the essential dynamic behaviour of the complete d-q dynamic model was chosen for the parametrization of the maximum torque per ampere (MTPA) cascade control (Li and Wang, 2019; Dianov *et al.*, 2022; Fontana and Bianchi, 2020).

In the presented analysis, the IPMSM was operated on the MTPA curve below base speed, where the MTPA curve obtained from the full nonlinear model was chosen to be the reference for control parameter identification. The proposed control parameter set was extracted based on the inductance maps by using the constant parameter MTPA equation, where curve fitting to the reference MTPA curve was performed. This set of parameters was tested using a MTPA control implementation and compared with two different sets of constant parameters that were chosen arbitrarily. Also, an array set of inductances that were extracted from the nonlinear MTPA line and were dependent on the current was used for the control. The dynamic performance of the four parameter sets was compared and analysed.

The aim of this paper was a systematic analysis of discussed influences through step-by-step reduction of the complexity of the dynamic model. This gives a deeper understanding of the behaviour of the machine and highlights the effects that are important to consider for speed control of the IPMSM. The paper presents how to determine adequate constant concentrated parameters of the d-q dynamic model for control in the MTPA operation and highlights the effect of different constant parameter sets on the dynamic behaviour of the control.

2. Theoretical background

2.1 IPMSM d-q dynamic model

The complete current-and position-dependent d-q dynamic model is presented in this section. The motion is described by:

$$J\frac{\mathrm{d}^2\theta_\mathrm{m}}{\mathrm{d}t^2} = T_\mathrm{e} - T_\mathrm{l} - k_\mathrm{f}\frac{\mathrm{d}\theta_\mathrm{m}}{\mathrm{d}t} - k_\mathrm{C}\left(\frac{\mathrm{d}\theta_\mathrm{m}}{\mathrm{d}t}\right)^2, \tag{1}$$

where J is the moment of inertia, k_f is the viscous friction coefficient, k_C is the ventilation coefficient, T_e is the electromagnetic torque and T_l is the load torque. The electrical position (angle) is $\theta = p\theta_\mathrm{m}$, where p is the number of pole pairs and θ_m is the mechanical rotor position. The voltage-balance equation in the d-q reference frame is given by:

$$\begin{bmatrix} u_{\mathrm{d}} \\ u_{\mathrm{q}} \end{bmatrix} = \begin{bmatrix} R & 0 \\ 0 & R \end{bmatrix} \begin{bmatrix} i_{\mathrm{d}} \\ i_{\mathrm{q}} \end{bmatrix} + \begin{bmatrix} L_{\mathrm{d,i}} & L_{\mathrm{dq,i}} \\ L_{\mathrm{qd,i}} & L_{\mathrm{q,i}} \end{bmatrix} \frac{\mathrm{d}}{\mathrm{d}t} \begin{bmatrix} i_{\mathrm{d}} \\ i_{\mathrm{q}} \end{bmatrix} + \frac{\mathrm{d}\theta}{\mathrm{d}t} \left(\begin{bmatrix} \frac{\partial \Psi_{\mathrm{d}}}{\partial \theta} \\ \frac{\partial \Psi_{\mathrm{q}}}{\partial \theta} \end{bmatrix} + \begin{bmatrix} 0 & -L_{\mathrm{q,a}} \\ L_{\mathrm{d,a}} & 0 \end{bmatrix} \begin{bmatrix} i_{\mathrm{d}} \\ i_{\mathrm{q}} \end{bmatrix} + \begin{bmatrix} 0 \\ \Psi_{\mathrm{md}} \end{bmatrix} \right), \tag{2}$$

$$\boldsymbol{L}_{\mathrm{i}} = \begin{bmatrix} \frac{\partial \Psi_{\mathrm{d}}}{\partial i_{\mathrm{d}}} & \frac{\partial \Psi_{\mathrm{d}}}{\partial i_{\mathrm{q}}} \\ \frac{\partial \Psi_{\mathrm{q}}}{\partial i_{\mathrm{d}}} & \frac{\partial \Psi_{\mathrm{q}}}{\partial i_{\mathrm{q}}} \end{bmatrix}, \boldsymbol{L}_{\mathrm{a}} = \begin{bmatrix} 0 & \frac{-\Psi_{\mathrm{q}}}{i_{\mathrm{q}}} \\ \frac{\Psi_{\mathrm{d}}}{i_{\mathrm{d}}} & 0 \end{bmatrix} \text{ and } \frac{\partial \boldsymbol{\Psi}}{\partial \theta} = \begin{bmatrix} \frac{\partial \Psi_{\mathrm{d}}}{\partial \theta} \\ \frac{\partial \Psi_{\mathrm{q}}}{\partial \theta} \end{bmatrix},$$

where i_d, i_a and u_{d}, u_{q} are the d-q reference frame voltages and currents, R is the resistance and Ψ_{q} is the flux linkage in the q-axis due to the current excitation. The total flux linkage in the d-axis is defined as $\Psi_{\mathrm{d}}^{*} = \Psi_{\mathrm{d}} + \Psi_{\mathrm{md}}$, where Ψ_{d} is the flux linkage in the d-axis due to the current excitation and Ψ_{md} is the flux linkage in the d-axis due to the permanent magnet. $L_{\mathrm{d,i}}$, $L_{\mathrm{dq,i}}$, $L_{qd,i}$ and $L_{\mathrm{q,i}}$ are the incremental inductances, as denoted by the subscript i, where $L_{\mathrm{d,a}}$ and $L_{\mathrm{q,a}}$ are the apparent inductances denoted by subscript a.

2.2 Reduced model's parameter identification

Three different parameter dependencies were constructed. Firstly, the dependencies of Ψ_{d}^{*}, Ψ_{q} and T_{e} from the position θ and the currents i_{d}, i_{q} were obtained by using an automated process. A MATLAB script was used to simulate different i_{d} and i_{q} combinations in a two-dimensional (2D) transient FEM model using Ansys Maxwell 2D. The calculated torque T_{e} (i_{d}, i_{q}, θ) was stored in a lookup table (LUT). Furthermore, the matrices of incremental inductances $\boldsymbol{L}_{\mathrm{i}}$ (i_{d}, i_{q}, θ), apparent inductances $\boldsymbol{L}_{\mathrm{a}}$ (i_{d}, i_{q}, θ) and position derivatives of the flux linkages $\frac{\partial \boldsymbol{\Psi}}{\partial \theta}$ (i_{d}, i_{q}, θ) were calculated. Figure 1 shows the workflow for the parameter identification approach.

In the second step, the average values of Ψ_{d}*, Ψ_{q} and T_{e} with respect to θ were considered to calculate current-dependent incremental inductances $\boldsymbol{L}_{\mathrm{i}}$ (i_{d}, i_{q}) and apparent inductances $\boldsymbol{L}_{\mathrm{a}}$ (i_{d}, i_{q}). The torque was defined as T_{e} (i_{d}, i_{q}). With this data, 2D and 3D LUTs were generated. In the third approach, $\boldsymbol{L}_{\mathrm{i}}$ and $\boldsymbol{L}_{\mathrm{a}}$ were considered current and position independent, whereas T_{e} was calculated according to:

$$T_{\mathrm{e}} = \frac{3}{2} p \left(\Psi_{\mathrm{md}} i_{\mathrm{q}} + i_{\mathrm{d}} i_{\mathrm{q}} \left(L_{\mathrm{d,a}} - L_{\mathrm{q,a}} \right) \right). \tag{3}$$

All other parameter values, such as R, J, k_{f}, k_{C}, p and Ψ_{md}, were assumed constant. A simulation was constructed in Simulink, by using equations (1) and (2) in combination with adequate LUTs. The model's inputs were u_{d}, u_{q} and T_{l}, whereas the outputs were i_{d}, i_{q}, T_{e} and θ and the phase currents i_{a}, i_{b} and i_{c}. In the third approach, equation (3) was used to determine the torque instead of the LUTs.

2.3 Overview of reduced models

By using the three presented approaches, five models were developed, equipped with specific features, terms and dependencies. Table 1 presents all five models, where M1 was

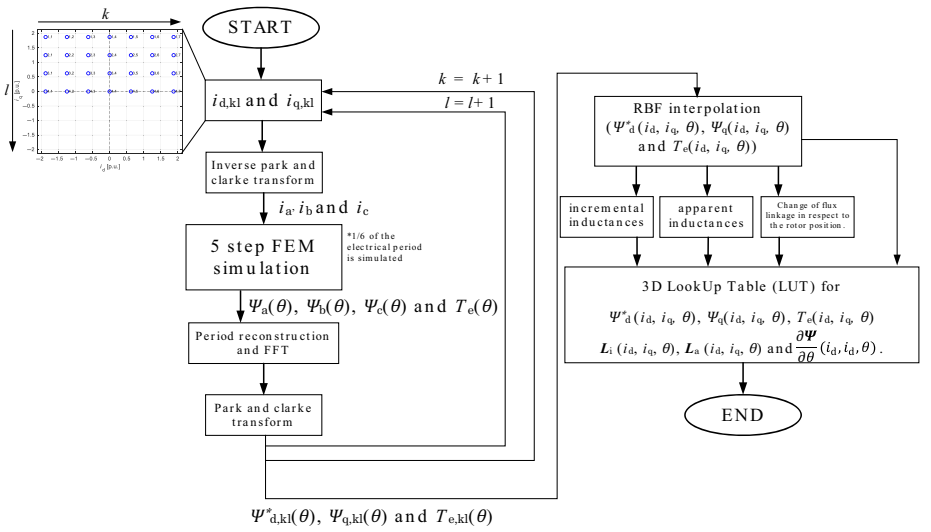

Figure 1. Workflow for the position and the current dependencies parameter identification

Model	Model features
M1	Defined by equations (1) and (2), parameters were dependent on θ, i_d and i_q. Torque LUT - $T_e(i_d, i_q, \theta)$
M2	M1 neglecting cross-saturation terms, i.e. $L_{dq,i}(i_d, i_q, \theta)$ and $L_{qd,i}(i_d, i_q, \theta)$
M3	M2 neglecting term $\frac{\partial \Psi}{\partial \theta}(i_d, i_q, \theta)$
M4	M3 neglecting θ dependence. Torque LUT - $T_e(i_d, i_q)$
M5	M4 with constant parameters that were operation point specific. Torque was defined by equation (3)

Table 1. Model complexity reduction from Model 1 to Model 5

the complete current- and rotor position-dependent d-q FEM-based reduced-order dynamic model. The complexity of reduced models was decreasing, where M5 was the simplest dynamic model with the constant parameters.

To evaluate the steady-state performance of the models, the motion equation (1) was neglected and the electrical angular velocity $\omega = \frac{d\theta}{dt}$ was chosen as an input for all five models. A representative operation point (OP) was defined by $u_d = -0.6$ p. u., $u_q = -0.9$ and $\omega = 1.3535$ p. u., referred to as OP1. All models were analysed in this OP. The constant parameters for M5 were obtained by using the steady-state i_d and i_q of M4 in OP1.

The higher harmonic content of M1, M2 and M3 was similar to the FEM model, which is presented in Figure 2 and Figure 3 when comparing the THD (i_a) and the torque ripple waveform of the three models versus the reference FEM results. By those metrics, M1 models the nonlinearities of the FEM model the most accurate. Furthermore, M4 and M5 had almost identical result of the current i_a and torque T_e in discussed comparison, as the steady-state i_d and i_q of M4 were used for obtaining the constant inductances of M5. The higher harmonics in M4 and M5 were very low, and there was no torque ripple, as the output was the mean torque. The difference between the rms(i_a) of FEM and M4 or M5 was 0.04%,

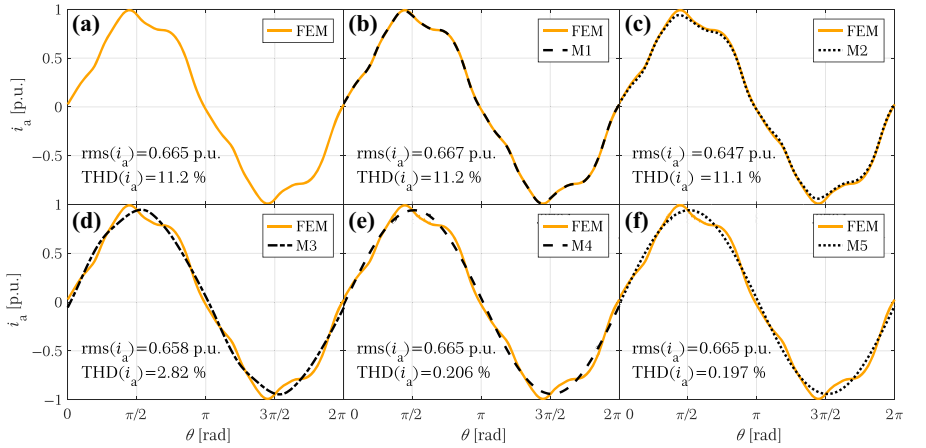

Figure 2.
The phase current in phase a of all five models compared with the results of the reference FEM model

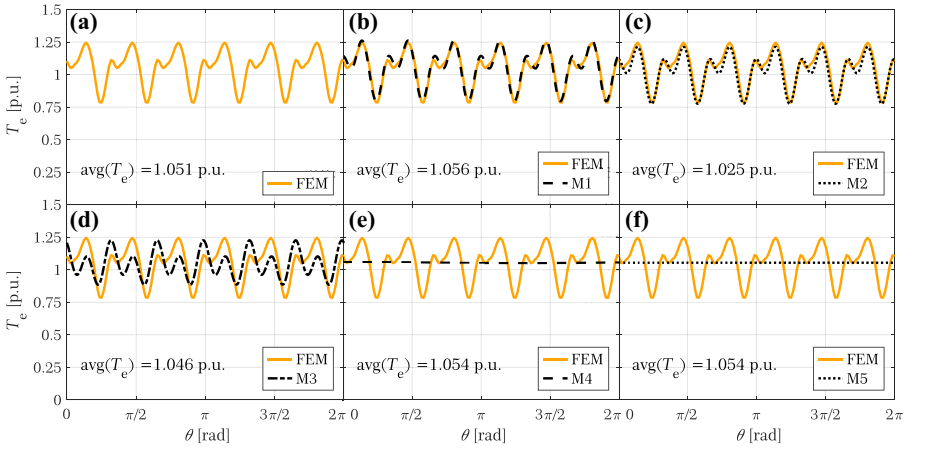

Figure 3.
The electromagnetic torque of all five reduced-order models compared with the FEM model

where the difference between the avg(T_e) between FEM and M4 or M5 was 0.3%, which was in both cases negligibly small.

2.4 Operation of reduced models

The dynamic behaviour and steady-state values at different OPs was compared between M1, M4 and M5. In this analysis, the motion equation (1) was included, where OP1 was simulated by applying a load torque $T_l = 1$ p. u. and voltage $u_d = -0.6$ p. u., $u_q = -0.9$ p. u. The operation was then changed to OP2 at 0.5 s with a load torque $T_l = 0.75$ p. u. and to OP3 at 1.5 s with $T_l = 1.25$ p. u. In Figure 4, the angular velocity ω and current i_d, i_q response to the change of the OPs are presented.

The stationary and dynamic behaviours of M1 and M4 in all three OPs were very similar for the current i_d, i_q and angular velocity ω response as presented in Figure 4. Steady-state values between the two models differ by less than 1%, as presented in Table 2. Only M5

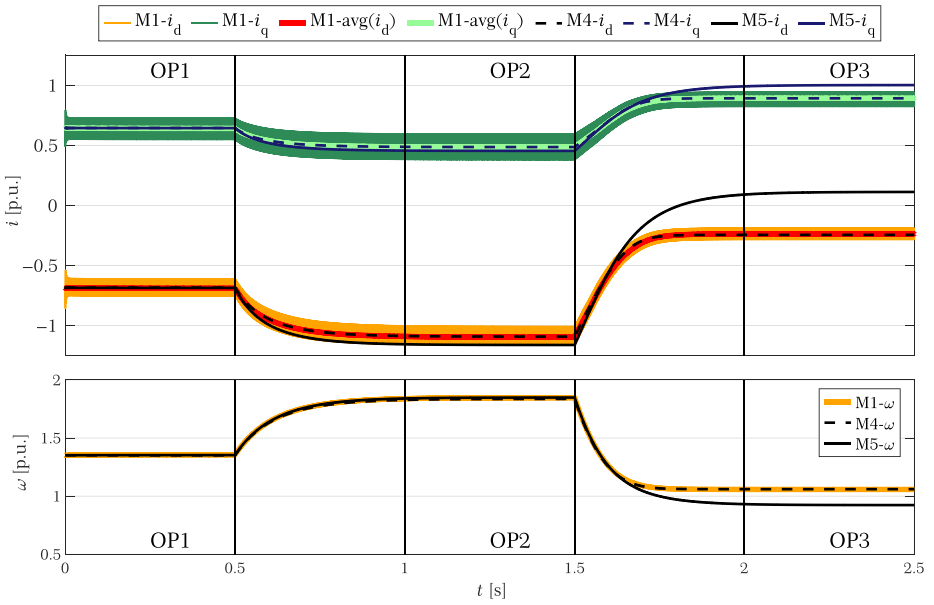

Figure 4. Angular velocity and current response of M1, M4 and M5 to the change of OPs

Quantity	OP1 M1	OP1 M4	OP1 M5	OP2 M1	OP2 M4	OP2 M5	OP3 M1	OP3 M4	OP3 M5
ω (p. u.)	1.3567	1.3510	1.3535	1.8475	1.8487	1.8368	1.058	1.0605	0.9235
Rel. diff. to M1	/	0.42%	0.24%	/	−0.07%	0.58%	/	−0.24%	12.7%
i_d (p. u.)	−0.692	−0.689	−0.687	−1.099	−1.095	−1.164	−0.240	−0.247	0.110
Rel. diff. to M1	/	0.47%	0.83%	/	0.39%	−5.94%	/	−2.81%	145.6%
i_d (p. u.)	0.639	0.643	0.642	0.484	0.484	0.452	0.890	0.890	0.997
Rel. diff. to M1	/	−0.59%	−0.39%	/	0.10%	6.66%	/	−0.03%	−12.1%

Table 2. Steady-state values and the relative difference to M1 of M4 and M5 for all three OPs

displays very different current i_d, i_q and angular velocity ω values and response for OP2 and OP3 compared with M1 (Table 2). The current i_d was 145% higher in the case of M5 compared with M1 in OP3, which accounted for the biggest difference.

M4 includes the current dependency of the apparent $\boldsymbol{L}_a$ (i_d, i_q) and incremental inductances $\boldsymbol{L}_i$ (i_d, i_q); consequently, those dependencies play a major role when modelling essential dynamic behaviour of the machine, for synthesis of the discussed cascade control. In Figure 5, the incremental inductance maps dependent on the current i_d and i_q of M4 are presented. On the maps, the discussed OPs are marked, and the values of the inductances are presented in Table 3.

The nonlinear and significant change of the inductances in different OPs has a major impact on the machine's behaviour and cannot be neglected and assumed constant. For example, the incremental inductances change in the q-axis from OP2 to OP3 for 26.6%. This also explains why M5 with constant parameter performed so different in OP2 and OP3 compared with the M4 and M1, as the parameters were identified based on the OP1. Therefore, the current dependency of the inductance was critical for the further development

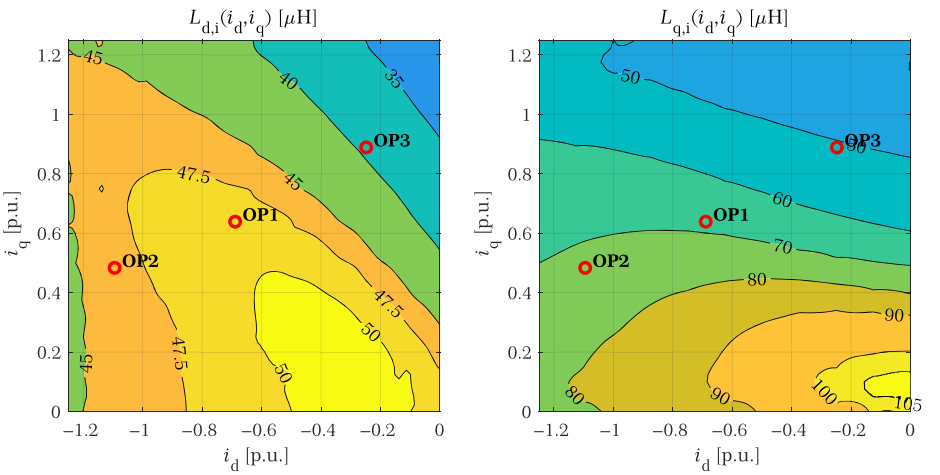

Figure 5.
Incremental inductance maps for M4 with highlighted OP1, OP2 and OP3

Table 3.
Inductance values at OP1, OP2 and OP3 for M4

			M4			
Operation points	i_d (p. u.)	i_q (p. u.)	$L_{d,a}$ (μH)	$L_{q,a}$ (μH)	$L_{d,i}$ (μH)	$L_{q,i}$ (μH)
OP1	−0.689	0.643	44.16	81.91	47.24	68.72
OP2	−1.095	0.484	46.70	77.47	46.64	71.85
OP3	−0.247	0.890	38.57	78.04	39.50	52.71

of control algorithms and must be considered. We can conclude that the position dependency, the terms $\frac{\partial \boldsymbol{\Psi}}{\partial \theta}$ and cross-saturation did not influence the discussed specific dynamic behaviour of the machine with the change of the OPs and have just a direct influence on the higher harmonic components of the currents and, consequently, a higher torque ripple.

2.5 Control parameter identification for MTPA control

A closed-loop cascade speed control was implemented for controlling the machine, which is based on constant parameters in the control algorithm (Dianov *et al.*, 2022). Proportional integral (PI) controllers were used for the speed and current control, and decoupling was added between the d- and q-axis voltage-balance equations. Feedforward MTPA control was implemented (Morimoto *et al.*, 1994; Rahman and Dwivedi, 2019). By using the presented implementation, the machine was operated only on the MTPA curve and below base speed.

For determining the constant inductance parameters, the M1 and M4 MTPA curves were extracted; however, they resulted in identical curves, as presented in Figure 6. To obtain the parameters for M5, curve fitting was performed on the reference M4 MTPA curve data, by using the MTPA equation:

$$i_d = \frac{\Psi_{md}}{2a} - \sqrt{\frac{\Psi_{md}^2}{4a^2} + i_q^2} \tag{4}$$

where the inductance difference $a = L_{q,a} - L_{d,a}$ was determined using the least squares method. The calculated value of a was 4.025 μH.

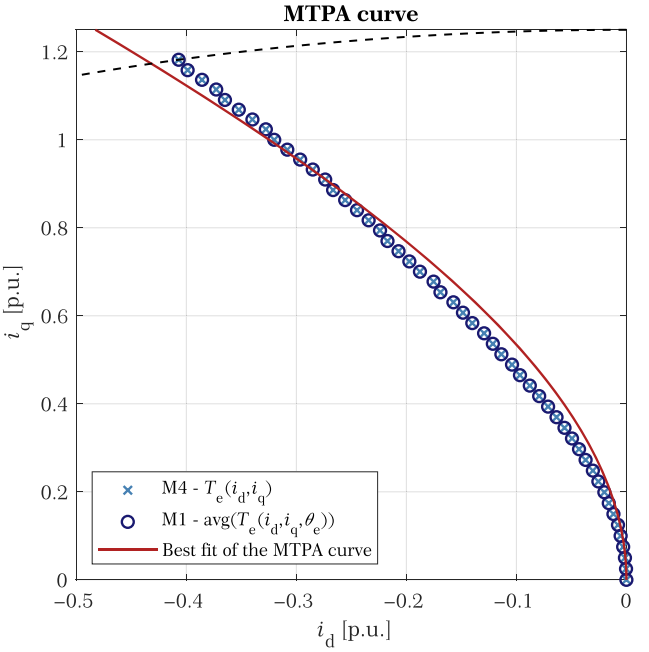

Figure 6.
Best fit of the constant parameter MTPA curve on the reference M4 MTPA curve data

The next step was to find the adequate inductance difference a on reference MTPA M4 curve. The inductances $L_{q,a}$ and $L_{d,a}$ were extracted from the inductance maps across the reference M4 MTPA curve (presented in Figure 8) and are presented in Figure 7 with respect to the total current $i = \sqrt{i_d^2 + i_q^2}$. The difference that matched the determined coefficient a between them was determined at a specific current, as presented in Figure 7a, and the inductances were determined at that point, as presented in Figure 7b. The values of the of inductances were $L_{q,a} = 78.95\ \mu H$ and $L_{d,a} = 38.7\ \mu H$.

Besides the parameter set ($L_{q,a}$ and $L_{d,a}$), referred to as set 3 (S3) and identified with the discussed method, two additional sets were determined for comparison reasons. The first set S1 was determined from the OP2, and the second set S2 was randomly chosen on the reference M4 MTPA curve (not with respect to the adequate a). All the chosen constant parameter sets are as follows:

- S1: apparent inductances from the OP2: $L_{q,a} = 77.47\ \mu H$ and $L_{d,a} = 46.70\ \mu H$;
- S2: random apparent inductances from the M4 MTPA curve: $L_{q,a} = 82.90\ \mu H$ and $L_{d,a} = 38.25\ \mu H$; and
- S3: apparent inductance fitted to the M4 MTPA curve: $L_{q,a} = 78.95\ \mu H$ and $L_{d,a} = 38.70\ \mu H$.

Finally, a vector parameter set (S4) of the apparent inductances was evaluated. The apparent inductances according to the reference M4 MTPA curve as a function of the total current i were chosen as control parameters and are denoted as follows:

- S4: $L_{q,a}(i)$ and $L_{d,a}(i)$.

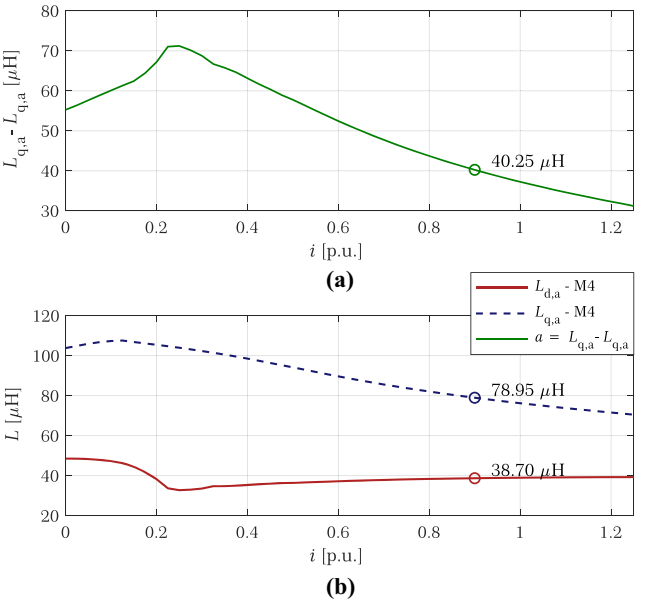

Figure 7.
Apparent inductances and their difference according to the reference M4 MTPA curve depending on the total current

All four parameter sets are presented on the apparent inductance map in Figure 8, where the change of the $L_{q,a}$ and $L_{d,a}$ can be observed according to the current change.

3. Results

The evaluation of the control parameters was performed based on M1 and an implementation of the cascade feedforward MTPA speed control algorithm. The apparent inductances were included in the following control parameters:

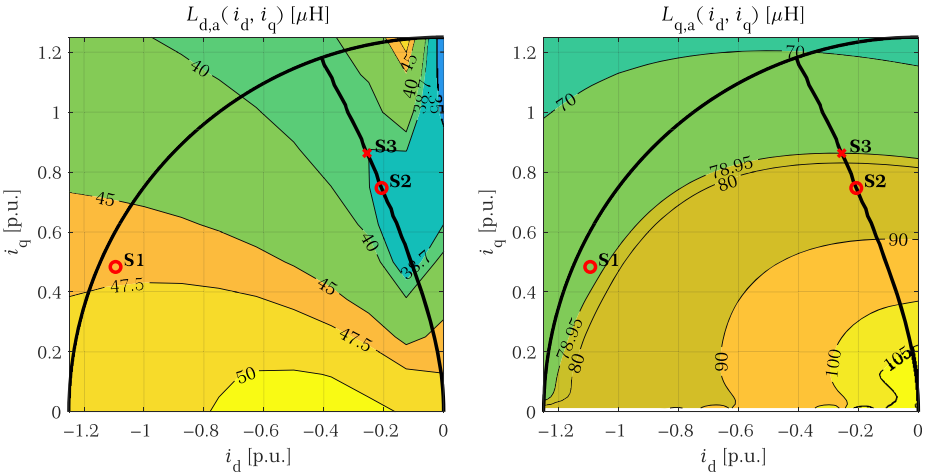

Figure 8.
Inductance maps for M4 with highlighted S1, S2, S3 and M4 MTPA curve

- time constant of current d- and q-axis PI regulator;
- time constant of speed PI regulator;
- decoupling; and
- MTPA control algorithm under base speed.

All other control parameters were assumed constant. The analysis of implemented control was performed using the following profile: first, the machine was started up to the reference angular velocity ω_{ref} and load torque T_1. When a steady-state operation was achieved, the load torque T_1 was increased. The control operation was described by:

$$\omega_{\text{ref}} = 0.9425 \text{ p.u. and } T_l(t) = \begin{cases} 0.75 & \text{p.u.}, \ t < 0.2 \ s \\ 1.25 & \text{p.u.}, \ t => 0.2 \ s \end{cases}$$

The responses of currents i_{d}, i_{q} and the angular velocity ω were analysed. Figure 9 shows the current i_{d}, i_{q} responses, and Figure 10 shows the angular velocity ω responses of the controlled machine for all four parameter sets.

The responses were stable in all four cases, and the reference angular velocity ω_{ref} was achieved. When evaluating the current responses in Figure 9, different dynamic responses between the models were observed. For the further analysis, the following performance indicators were calculated:

- M_{s} – steady-state value;
- t_{s} – settle time;
- $e\%$ – relative overshoot;
- integral square error or ISE $= \int_0^T e(t)^2 \text{d}t$, where e (t) is the difference to the steady-state value; and
- integral absolute error or IAE $= \int_0^T |e(t)| \text{d}t$.

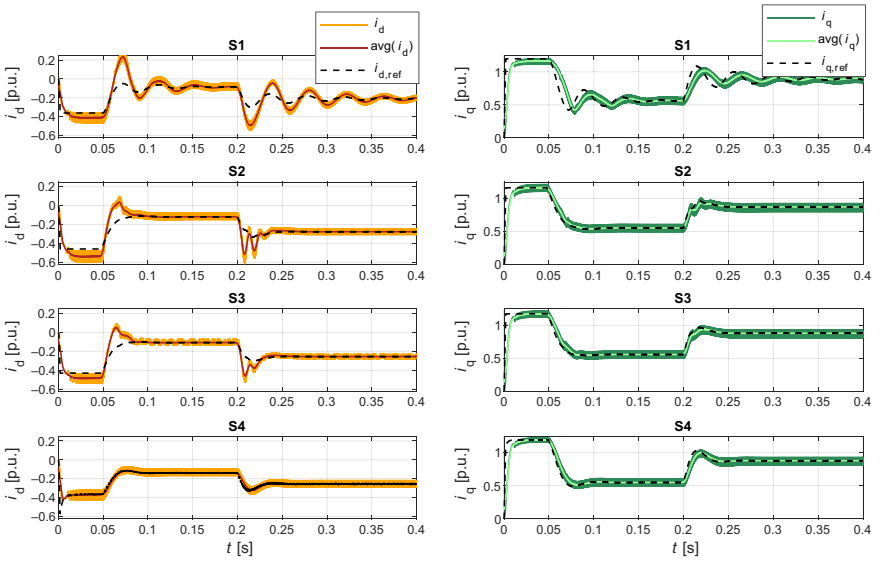

Figure 9. i_{d} and i_{q} dynamic response to a load torque T_1 step for S1, S2, S3 and S4

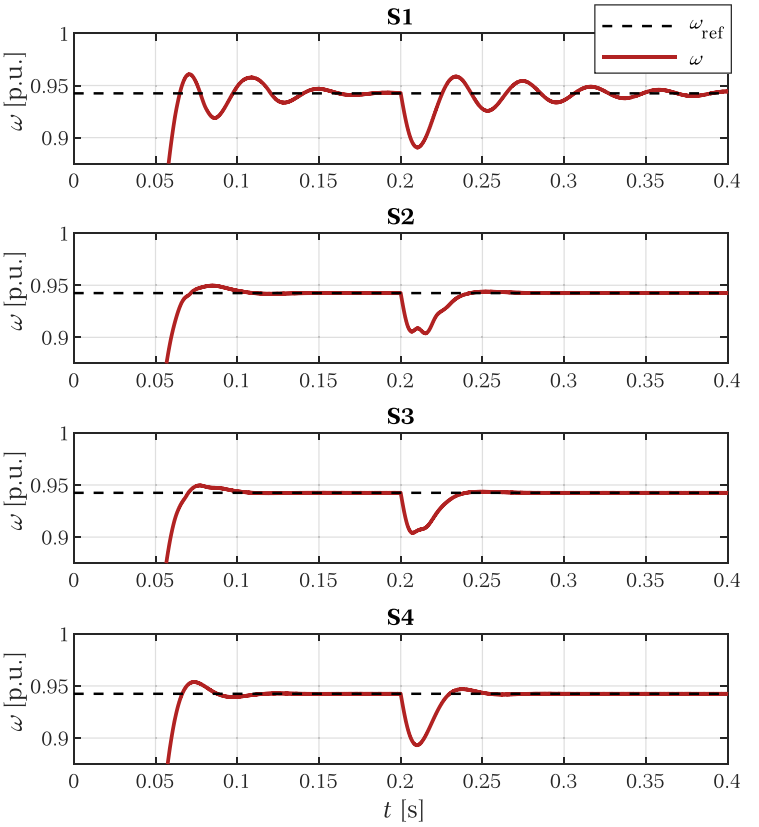

Figure 10.
ω dynamic response to a load torque step T_1 for S1, S2, S3 and S4

For all four parameter sets and for two load torques T_1 applied, the performance indicators were calculated, as presented in Table 4. The least adequate control performance was achieved with S1, where the performance indicators were the highest almost in all cases. When comparing just the constant parameter sets, S3 that was calculated by fitting the reference M4 MTPA curve outperformed S1 and S2. The settling time t_s of S2 and S3 had similar values, whereas S1 in the case of i_d and $T_1 = 1.25$ p. u. did not reach the steady-state value. When comparing the S4 response with the S3 response, it performed better in the case of the current response in the d-axis i_d, where the angular velocity ω and the current in the q-axis i_q responded better to S3, as presented in Table 4.

When analysing the steady-state currents i_d and i_q shown in Table 4 of the S4 current-dependent parameters, they produce at all load torques T_1, the optimal nonlinear MTPA point, as expected, as the M4 and M1 MTPA curves align perfectly, as shown in Figure 6. The biggest difference of i_d and i_q to the M4 MTPA values was observed for the parameters of S1, where in the case of i_d and $T_1 = 0.75$ p. u., the difference was 38%. The lowest difference at $T_1 = 0.75$ p. u. of i_d and i_q to the M4 MTPA values was observed for the parameters of S2. The lowest difference at $T_1 = 1.25$ p. u. of i_d and i_q to the M4 MTPA values was observed for the parameters of S3. This was because both parameter sets of S2 and S3 give different MTPA approximations and

	S1		S2		S3		S4	
Quantity	$T_1 = 0.75$ p. u.	$T_1 = 1.25$ p. u.	$T_1 = 0.75$ p. u.	$T_1 = 1.25$ p. u.	$T_1 = 0.75$ p. u.	$T_1 = 1.25$ p. u.	$T_1 = 0.75$ p. u.	$T_1 = 1.25$ p. u.
i_d [p. u.] – M_s	−0.86	/(−0.209)	−0.118	−0.276	−0.109	−0.257	−0.139	−0.254
i_q [p. u.] – M_s	0.563	0.892	0.555	0.873	0.557	0.879	0.551	0.880
ω [p. u.] – M_s	0.943	0.943	0.943	0.943	0.943	0.943	0.943	0.943
i_d [p. u.] – t_s	0.22	/	0.13	0.067	0.12	0.062	0.11	0.054
i_q [p. u.] – t_s	0.18	0.20	0.11	0.48	0.11	0.045	0.11	0.052
ω [p. u.] – t_s	1.56	0.16	0.1	0.037	0.1	0.034	0.10	0.045
$i_d - e$%	452.07	159.65	407.69	121.67	404.12	108.26	212.72	43.42
$i_q - e$%	112.49	18.87	118.17	15.43	117.63	12.54	122.39	18.02
$\omega - e$%	1.95	1.72	0.74	0.14	0.76	0.10	1.20	0.47
i_d –ISE	10.36	2.77	13.09	1.01	10.99	0.71	4.92	0.19
i_q –ISE	32.68	1.85	29.56	0.84	30.63	0.83	33.54	1.13
ω –ISE	$3.56\ 10^5$	642.64	$3.49\ 10^5$	397.8	$3.47\ 10^5$	359.16	$3.53\ 10^5$	497.90
i_d –IAE	1.03	0.57	0.93	0.16	0.86	0.14	0.58	0.08
i_q –IAE	1.68	0.42	1.42	0.14	1.44	0.13	1.50	0.18
ω –IAE	132.26	6.67	126.53	3.39	126.29	3.09	128.43	3.52

Table 4.
Dynamic response performance indicators of S1, S2, S3 and S4

were closer to the nonlinear MTPA curve of model M1 in different OPs, defined by the load torque T_1. Constant parameters for control purposes must be chosen according to a criterion, as the results showed that the two arbitrarily chosen parameter sets S1 and S2 performed worse compared with S3. The criterion chosen in these analyses was to fit the nonlinear M4 MTPA curve with constant inductances. Adequate results can be also achieved with a vector set of the inductances changing with respect to the current along the MTPA curve.

4. Conclusion

The nonlinear FEM model was used to extract the inductance matrices $\boldsymbol{L}_{\mathrm{i}}$, $\boldsymbol{L}_{\mathrm{a}}$ and position derivatives of the flux linkages $\frac{\partial \boldsymbol{\Psi}}{\partial \theta}$ with respect to the current i_{d}, i_{q} and position θ change. A reduced-order dynamic model was developed, which very accurately modelled the FEM model. The model was step-by-step reduced to the current-dependent M4 and the constant parameter M5. M4 modelled the essential dynamic behaviour of the nonlinear FEM-based M1, where the M5 showed a big deviation compared with the M1 when not operating in the specific operation point for which its parameters were determined. It was concluded that the current-dependent M4 can be further used for control development and the θ dependency and the neglected additional terms did not affect the dynamic behaviour. Furthermore, a reference M4 MTPA nonlinear curve was extracted, where a curve fit was performed with the constant parameter MTPA equation to obtain the constant apparent inductances from the inductance maps for S3. S3 was evaluated on a cascade MTPA speed control versus two arbitrarily chosen parameter sets (S1 = OP2 and S2 = random from the M4 MTPA curve). Additionally, the inductances across the reference M4 MTPA array in dependency from the total current i were implemented. The dynamic response performance indicators showed that the least adequate parameters were the ones from S1. The most adequate parameters were from S3, as they performed better than the constant S1 and S2 parameters and gave better responses of the current in the d-axis i_{d} and the angular velocity ω compared with S4. The S4 parameter achieved at each load torques T_1 the optimal nonlinear MTPA point. The results show that the proposed method for extracting the constant parameters gives adequate results and can be used in applications where the parameters for MTPA operation are limited to constant values, despite the IPMSM being highly nonlinear.

References

Dianov, A., Tinazzi, F., Calligaro, S. and Bolognani, S. (2022), "Review and classification of MTPA control algorithms for synchronous motors", *IEEE Transactions on Power Electronics*, Vol. 37 No. 4, pp. 3990-4007, doi: 10.1109/tpel.2021.3123062.

Fontana, M. and Bianchi, N. (2020), "Design and analysis of normal saliency IPM spoke motor", *IEEE Transactions on Industry Applications*, pp. 1-1, doi: 10.1109/tia.2020.2988842.

Hadžiselimović, M., Štumberger, G., Štumberger, B. and Zagradišnik, I. (2007), "Magnetically nonlinear dynamic model of synchronous motor with permanent magnets", *Journal of Magnetism and Magnetic Materials*, Vol. 316 No. 2, pp. e257-e260, doi: 10.1016/j.jmmm.2007.02.114.

Li, K. and Wang, Y. (2019), "Maximum torque Per ampere (MTPA) control for IPMSM drives based on a variable-equivalent-parameter MTPA control law", *IEEE Transactions on Power Electronics*, Vol. 34 No. 7, pp. 7092-7102, doi: 10.1109/tpel.2018.2877740.

Liu, X., Chen, H., Zhao, J. and Belahcen, A. (2016), "Research on the performances and parameters of interior PMSM used for electric vehicles", *IEEE Transactions on Industrial Electronics*, Vol. 63 No. 6, pp. 3533-3545, doi: 10.1109/tie.2016.2524415.

Lu, H., Li, S., Feng, B. and Li, J. (2022), "An enhanced sensorless control based on active disturbance rejection controller for a PMSM system: design and hardware implementation", *Assembly Automation*, Vol. 42 No. 4, doi: 10.1108/aa-01-2022-0016.

Michalski, T., Acosta-Cambranis, F., Romeral, L. and Zaragoza, J. (2019), "Multiphase PMSM and PMaSynRM flux map model with space harmonics and multiple plane cross harmonic saturation", paper presented at the IECON 2019 - 45th Annual Conference of the IEEE Industrial Electronics Society, 14-17 October, Lisbon, Portugal, available at: https://ieeexplore.ieee.org/document/8927421 (accessed: 2022-03-03T07:30:10).

Morimoto, S., Sanada, M. and Takeda, Y. (1994), "Wide-speed operation of interior permanent magnet synchronous motors with high-performance current regulator", *IEEE Transactions on Industry Applications*, Vol. 30 No. 4, pp. 920-926, doi: 10.1109/28.297908.

Müller, F., Baumanns, P., Nell, M.M. and Hameyer, K. (2022), "Nonlinear parametric simulation by proper generalized decomposition on the example of a synchronous machine", *COMPEL – The International Journal for Computation and Mathematics in Electrical and Electronic Engineering*, Vol. 41 No. 4, doi: 10.1108/compel-11-2021-0431.

Pouramin, A., Dutta, R., Rahman, M.F. and Xiao, D. (2015), "Inductances of a fractional-slot concentrated-winding interior PM synchronous machine considering effects of saturation and cross magnetization", paper presented at the 2015 IEEE Energy Conversion Congress and Exposition (ECCE), 20-24 September, Montreal, Canada, available at: https://ieeexplore.ieee.org/document/7310511 (accessed: 2022-02-16T18:48:29).

Rafaq, M.S. and Jung, J.-W. (2020), "A comprehensive review of state-of-the-Art parameter estimation techniques for permanent magnet synchronous motors in wide speed range", *IEEE Transactions on Industrial Informatics*, Vol. 16 No. 7, pp. 4747-4758, doi: 10.1109/tii.2019.2944413.

Rahman, M.F. and Dwivedi, S.K. (2019), *Modeling, Simulation and Control of Electrical Drives*, Institution of Engineering and Technology.

Stumberger, B., Stumberger, G., Dolinar, D., Hamler, A. and Trlep, M. (2003), "Evaluation of saturation and cross-magnetization effects in interior permanent-magnet synchronous motor", *IEEE Transactions on Industry Applications*, Vol. 39 No. 5, pp. 1264-1271, doi: 10.1109/tia.2003.816538.

Weidenholzer, G., Silber, S., Jungmayr, G., Bramerdorfer, G., Grabner, H. and Amrhein, W. (2013), "A flux-based PMSM motor model using RBF interpolation for time-stepping simulations", paper presented at the 2013 International Electric Machines & Drives Conference, 12- 15 May, Westin O'Hare, Chicago, IL, available at: https://ieeexplore.ieee.org/document/6556323 (accessed: 2021-02-02T08:12:04).

Zhu, Z.Q., Liang, D. and Liu, K. (2021), "Online parameter estimation for permanent magnet synchronous machines: An overview", *IEEE Access*, Vol. 9, pp. 59059-59084, doi: 10.1109/access.2021.3072959.

About the authors

Mitja Garmut received his MSc degree in electrical engineering from the University of Maribor, Maribor, Slovenia, in 2020. He is currently working as a researcher at the Faculty of Electrical Engineering and Computer Science, University of Maribor. His current research interests include optimization, modelling and control of electrical machines in the electromagnetic, thermal and mechanical fields. Mitja Garmut is the corresponding author and can be contacted at: mitja.garmut@um.si

Simon Steentjes received the Diploma and Dr Ing. degrees in electrical engineering from RWTH Aachen University, Germany, in 2011 and 2017, respectively. He has been a research

associate and the group leader of the Institute of Electrical Machines (IEM), RWTH Aachen University, from 2011 to 2018. He is currently leading the Electric-Motor-Development Group with Hilti Entwicklungsgesellschaft GmbH, Kaufering. His research interests include hard- and soft-magnetic material modelling, iron-loss calculation, effects of material processing and thermal effects in electrical machines.

Martin Petrun received his BSc and PhD degrees in electrical engineering from the University of Maribor, Maribor, Slovenia, in 2010 and 2014, respectively. He is currently working as a researcher and an associate professor at the University of Maribor. His current research interests include modelling of dynamic phenomena inside soft magnetic materials as well as modelling and control of electrical and electromechanical converters and power electronics.